UNIVERSITY OF LATVIA

Summary of Doctoral Thesis

Kaspars Kaprāns

THE STUDY OF TRANSITION METAL OXIDE ELECTRODE MATERIALS FOR APPLICATIONS IN LITHIUM-ION BATTERIES

Riga 2024

UNIVERSITY
OF LATVIA

FACULTY OF PHYSICS, MATHEMATICS AND OPTOMETRY

Kaspars Kaprāns

THE STUDY OF TRANSITION METAL OXIDE ELECTRODE MATERIALS FOR APPLICATIONS IN LITHIUM-ION BATTERIES

SUMMARY OF THE DOCTORAL THESIS

Submitted for the degree of Doctor of Science (Ph. D.)
in Natural Sciences in Physics and Astronomy

Subfield: Physics of Materials

Riga 2024

The doctoral thesis was carried out at the Institute of Solid - State Physics, University of Latvia, from 2015 to 2023.

The thesis contains an introduction, four chapters, conclusions, and a reference list.

Type of thesis: dissertation in Physics and Astronomy in the subfield physics of materials.

Supervisor: *Dr.chem*. **Gunārs Bajārs**, a leading researcher at the Institute of Solid-State Physics, University of Latvia

Reviewers:

1) **Māris Knite ,** *Dr. habil. Phys.,* professor, Riga Technical University;
2) **Andris Šutka,** *Dr. Phys.,* professor, Riga Technical University;
3) **Tomas Salkus,** *Dr.,* professor, University of Vilnius, Lithuania.

The thesis will be defended at the public session Doctoral Committee of Physics and Astronomy, University of Latvia, at 15:00 on April 19th, 2024, in the conference hall of the Institute of Solid-State Physics, University of Latvia, Kengaraga Street 8, Riga.

The thesis and its summary are available at the Library of the University of Latvia, Raina blvd. 19.

Chairman of the Doctoral Committee _____ / *Dr. habil. phys. Linards Skuja* /
(Signature)

Secretary of the Doctoral Committee _____/ *Sintija Siliņa* /
(Signature)

ISBN 978-9934-36-201-9
ISBN 978-9934-36-202-6 (PDF)

ABSTRACT

The electrode materials of iron oxide, titanium dioxide and reduced graphene oxide (rGO) for lithium-ion batteries were investigated by electrophoretic deposition and their applicability was evaluated.

A composition, structure and morphology of the electrode materials were investigated by scanning electron microscopy, atomic force microscopy, X-ray diffraction analysis, Raman spectroscopy, X-ray microspectral analysis and X-ray photoelectron spectroscopy.

Ternary Fe_2O_3/TiO_2/rGO anode material showed better electrochemical performance compared to the binary Fe_2O_3/rGO and TiO_2/rGO electrodes. Obtained gravimetric capacities at the discharge current 0.5 mA are 571, 683, 729 mAh/g for the respective nanocomposite electrode materials Fe_2O_3/TiO_2 in molar ratios of 1:1 (FT11), 2:1 (FT21) and 3:1 (FT31). After 400 charge-discharge cycles at the current value 1 mA, the nanocomposites retains 58 %, 81 % and 17 % of its initial gravimetric capacity for FT11, FT21 and FT31, respectively. Based on the results of rate capability, cyclability and gravimetric capacity measurements, the nanocomposite with a molar ratio of Fe_2O_3 to TiO_2 (2:1) is a promising high performance electrode material for lithium-ion batteries.

The results obtained in this work extend understanding about interaction between two transition metal oxides for the preparation of high performance electrode materials for lithium-ion batteries by using a cheap, simple and environmentally friendly method. The possibility to adjust a properties of electrode material (rate capability, gravimetric capacity, cyclability) makes it promising for lithium-ion battery applications such as laptops, power tools, smartphones, drones, electric cars, etc.

Keywords: electrode material, electrophoretic deposition, transition metal oxides, lithium-ion battery, charge-discharge.

TABLE OF CONTENTS

1. INTRODUCTION

1.1. Relevance and motivation

The words "global warming" and "alternative energy" in human consciousness are associated with wind turbines or vast solar fields, but today the question of how to store, not just produce, environmentally friendly energy is becoming more and more pressing. The rapidly growing market for portable electrical devices and the emergence of green thinking make research in this area so relevant [1]. A lithium-ion battery (LIB) is a rechargeable electrical energy storage device. It consists of two electrodes, a cathode and an anode, an electrolyte, a separator and an integrated safety chip to avoid damage to the battery in case of overcharging or overly rapid discharge [2]. Transition metal oxides are characterised by a high theoretical charge capacity due to a conversion-type reaction during the lithiation of the electrode material; however, electrochemical cycling of the electrode leads to irreversible changes in the crystal structure of the material, leading to a rapid and irreversible decrease in charge capacity [3]. Since electrical conductivity is also an important property of the LIB electrode material and transition metal oxides are generally poor conductors of electrons, an electron conducting material (carbon or its allotropic form) is also included in the synthesis of the composite material. Combining materials with significant gravimetric charge capacity, high mechanical strength and good electrical conductivity can lead to new LIB electrode materials that can significantly improve the electrochemical performance of the battery [8-9].

Electrophoretic deposition (EPD) is the movement of charged particles in a colloidal solution induced by an external electric field and deposited on an electrically conductive substrate to form a thin film of material. Compared to other thin-film methods, it is cheap, simple and does not use toxic chemicals. As far as the thin-film process is concerned, it is worth mentioning that the method allows easy control thin-film morphology and thickness by varying the electrodeposition time and the magnitude of the electric field [7].

In this work, electrodeposited composite films consisting of two transition metal oxides (Fe_2O_2, TiO_2) and reduced graphene oxide (rGO) as a conductive additive were studied. The iron oxide is characterised by a high theoretical charge capacity (1006 $mAhg^{-1}$) but poor electrochemical cycling stability. Since the volume change of TiO_2 crystal lattice during lithiation of the electrode material is ≈ 4 % and it is characterised by high electrochemical cycling stability, TiO_2 was used to ensure the electrochemical cycling stability of the investigated composite electrode [3]. Currently, common methods such as thermal alloying [4], hydrothermal synthesis [5], chemical synthesis [6], atomic layer deposition [7] and chemical vapour deposition [8] are used to synthesise LIB electrode materials. Despite their widespread use, these methods have some serious drawbacks:

1. Their use requires large economic resources.
2. Heating at high temperatures (T > 1000 K) can damage the structure of the electrode material, increasing its brittleness, resulting in a loss of electrical contact between the active material and the conductive substrate.
3. Electrode material synthesis requires expensive, large and complex equipment.
4. The electrode material synthesis process is time-consuming.
5. The use of substrate materials for the active electrode material which are not resistant to high temperatures and pressures is not possible.
6. Limited choice of geometrical shape of the conductive substrate, which is related to the characteristics of the equipment to be used.

7. The substances used are highly volatile and toxic.

In order to synthesize electrode materials, the electrophoretic deposition (EPD) was used. Main advantages of EPD are:

1. Reduced (5-10 min) synthesis time of the electrode material.
2. Electrophoretic deposition requires only a DC power supply and two electrodes placed in suspension;
3. No limitation on the geometrical dimensions of the substrate.
4. No binder required.
5. No toxic substances are used and no hazardous waste is generated.
6. The EPD method is cost-effective and easy to apply.
7. The thickness and morphology of the resulting material layer can be controlled by varying EPD process parameters such as the magnitude of the external electric field and the deposition time.

The use of electrophoretic deposition in the synthesis of electrode materials significantly reduces the cost of LIB production and makes the production process "greener". The EPD method speeds up the production process of electrode materials and avoids the production of hazardous waste, which is an important environmental factor. Electrophoretically deposited composite electrode material Fe_2O_3/TiO_2/rGO combines two important properties for a lithium-ion battery: high gravimetric charge capacity and long-term stability of the lithium-ion battery during multiple charge-discharge cycles.

1.2. Aim and objectives

The aim of this work is to obtain Fe_2O_3, TiO_2 and reduced graphene oxide composite films by electrophoretic deposition. To study their physical and electrochemical properties depending on the slurry composition and to evaluate their applicability in lithium-ion batteries. In order to achieve the aim of this work, following objectives have been set:

1. To obtain rGO, Fe_2O_3/rGO and TiO_2/rGO thin films by electrophoretic deposition.
2. To synthesize nanocomposite films with different molar ratios of transition metal oxides and reduced graphene oxide as conductive additive by electrophoretic deposition.
3. Study and compare the composition, structure and morphology of the obtained nanocomposite films.
4. Determine the charge capacity of the electrode materials and evaluate the kinetics of the charge-discharge process.
5. Evaluate the results and predict the applicability of the composite material in lithium-ion batteries.

1.3. Author contribution

The author has done:

1. Electrophoretic deposition of nanocomposite films, analysis and preparation of suspensions and obtained all material films studied in the work.
2. X-ray diffraction measurements of all obtained materials and quantitative phase composition assessment of nanocomposite materials using Rietveld method.
3. Assembly of the battery half-cells, performing of the measurements and analysis of the results. The author has independently mastered and applied the modelling of electrochemical impedance spectra and interpretation of the obtained data. The author of the paper is the first and corresponding author of two scientific publications in cited journals about the doctoral thesis.

1.4. Scientific novelty

In this work, the electrochemical properties of a three-component Fe_2O_3/TiO_2/rGO electrode are studied in depth and the battery performance is analysed depending on the molar concentration of Fe_2O_3 and TiO_2. Among the materials, the best electrode composition was found, which provides both high charge capacity and stability during the multiple charge - discharge process. For the first time, nanocomposite films of iron oxide, titanium dioxide and graphene oxides were obtained by electrophoretic deposition and the potentiality of electrode material for applications in lithium-ion batteries was evaluated depending on the composition of the suspension.

1.5. Thesis structure

The “Theory and Literature Review” chapters of the thesis review the theory and literature on battery design, operating principles and physical parameters related to battery. The most common cathode and anode materials are also discussed. It provides an overview of charge storage processes and describes the role of the electrode-electrolyte interface in battery performance.

The chapter “Experimental part” gives an insight into the procedure and methodology used for the synthesis of the composite film samples and describes obtained materials more detail.

The practical results are summarised in the 2 subsections of the “Results and Discussion” chapter:

1. Study of electrophoretically deposited iron oxide, titanium dioxide and reduced graphene oxide as electrode material.
2. Studies of different quantitative compositions iron oxide and titanium dioxide electrode materials.

The final part summarizes conclusions, theses, and the author's publicity.

2. THEORY AND LITERATURE REVIEW

2.1. Battery design and operation

A battery is a device that directly converts the chemical energy stored in its active materials into electrical energy through oxidation-reduction reactions. There are two types of battery: primary and secondary. Primary batteries can convert their chemical energy into electrical energy only once, while secondary batteries are designed for multiple charge-discharge cycles. The boundary between primary and secondary batteries is not clear, as many primary batteries can be recharged repeatedly under certain conditions, but they are not very stable. In this work the composite material of transition metals and reduced graphene oxide is studied as an anode material for secondary batteries, so the word battery in the context of this work will be understood as a secondary battery or a rechargeable battery. A battery consists of electrochemical cells connected in series [1]. Electrodes are defined as a cathode (positive electrode) and an anode (negative electrode) which are placed in an electrolyte, an ion-conducting (electron-blocking) substance, usually in a liquid or solid aggregate state. The electrodes are separated from each other by a separator. Depending on whether the battery is being charged or discharged, one electrode undergoes an oxidation reaction (electron removal), the other simultaneously a reduction reaction (electron addition). When the external circuit is closed, ions move between the electrodes through the electrolyte, while electrons move in the external circuit. The flow of electrons in the external circuit provides a current to which an electrical consumer can be connected (**see Figure 2.1).**

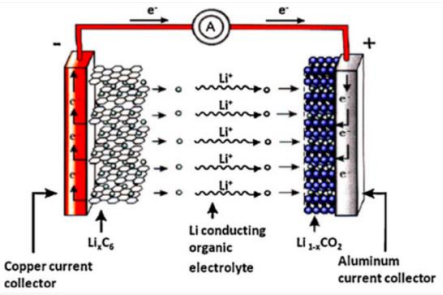

Figure 2.1. Simplified battery discharge process [2]

During battery operation, lithium ions flow between the electrodes in the electrolyte under the influence of an external electric field, which, through intercalation and/or conversion reactions, couple to the respective electrode, while an electric current - electrons - flows in the external circuit of the battery. For this reason, LIBs belong to the 'rocking chair battery'. The name is derived from the way the Li^+ cations move ('rock') between the electrodes. As the ions do not adsorb on the electrode surface but intercalate (insert) into the electrodes, the formation of dendrites (electrode surface artefacts) and thus the undesirable risk of electrochemical cell short-circuiting is avoided.

2.2. Anode materials

The first negative electrode or anode material used in lithium-ion batteries was metallic lithium, mainly because of its high gravimetric charge capacity (3800 $mAhg^{-1}$). Lithium ions are able to move through the passivating layer of the electrode surface during discharge, but tend to form dendrites (icicle-like growths) on the surface of the lithium electrode during charging, which can cause electrical contact between the cathode and anode, leading to a short circuit. This led to the need to look for other anode materials with a lower chemical potential than lithium metal. Graphite, with a Fermi energy only about

0.5 eV lower than that of lithium, proved to be a good material for this purpose. Lithium can reversibly intercalate into graphite to form the LiC_6 compound [10]. The search for an efficient anode material is not limited to carbon and lithium, but also amorphous silicon [11], Si nanowires [12], Si composites [13-14], titanium dioxide [15] and its nanowires [16]. Studies on the effect of carbon compounds on iron oxide anode material concluded that the mass fraction of carbon additives plays a significant role in the variation of cyclability, charge capacity and conductivity of the battery cell [17]. Graphene combined with iron oxide reduces the internal resistance of the battery and shortens the diffusion path of lithium ions and inhibits the agglomeration of iron oxide grains, thus preventing charge capacity reduction and material pulverisation during lithiation-delithiation. During battery operation, repeated charge-discharge cycles cause microscopic volume fluctuations in the anode material, leading to degradation and pulverisation. The addition of graphene or rGO reduces the effect of these factors on the electrochemical performance of the battery [18]. The reasons for forming composite materials when synthesising new anode materials are to combine their positive properties, which contribute to improving and developing the overall electrochemical performance of the battery.The literature review concluded that the three-component electrode materials show better overall battery performance compared to the performance of each individual electrode material.

Intercalation, impurity and conversion reactions are the three basic mechanisms that dominate energy storage in LIBs. Typical intercalation anode materials (graphite, TiO_2 , etc.) are characterised by one or more ion transport channels that allow intercalation of lithium ions without significant changes in the material structure. In the case of addition, a bond is formed between the lithium ion and an atom (A) of the base material, e.g. Si, Ge, Sn, forming a Li-A solids mixture. A conversion-type energy storage reaction occurs when the lithium ion binds to a binary material (MX), where M is the transition metal (Fe, Co, Cu) and X is the oxidant (O, S, F). In the process, the metal (M) cation is reduced to M^0 and LiX is simultaneously formed as a side-product of the reaction [19].

2.3. Cathode materials

Much of the research in lithium-ion battery development has focused on the search for a suitable cathode material to facilitate lithium ion injection and extraction at high potentials (4 V vs. Li/Li^+) [20]. The cathode is the positive electrode of the battery on which the reduction reactions take place during discharge. Aluminium is commonly used as a current collector in cathode studies due to its high oxidation potential (4.7 V vs. Li/Li^+) and therefore electrochemical stability. The cathode performance depends on the morphology, microstructure and electrochemical properties of the material used. Energy storage is provided by two main mechanisms: intercalation and conversion. In the intercalation process, the cathode material acts as a 'trapping network' for the lithium ions, which penetrate into the atomic space and deposit between the layers of the material. Conversion-type energy storage is a solid-state reduction-oxidation reaction in which crystal lattice changes occur with subsequent chemical bond breakage and recombination. The significant volume change of electrode material during lithiation-delithiation and the poor electron conductivity in development of conversion-type cathode materials still remain a major challenge for researchers.

Cathode materials are divided into three categories according to the type of energy storage: calcogenides, transition metal oxides and polyanion composites. Most research has focused on transition metal oxides due to their high energy storage capacity [21]. According to their structure, cathode materials are divided into *olivine*, *layered* and *spinel* types. The layered structure $LiCoO_2$ (LCO) is one of the most commonly used cathode materials, however it is not convenient for large batteries as the use of large amounts of cobalt in energy storage devices is not economically viable. Spinel-type cathode materials are widespread, with AB_2O_4 being the characteristic structural form and $LiMn_2O_4$ (LMO) being the most widely used cathode material in this group. One of the main advantages compared to other types is the high stability of the spinel structure over repeated charge-discharge cycles, but a disadvantage is the high sensitivity to temperature changes in the external environment. LFP or $LiFePO_4$

olivine-type polyanionic cathode materials continue to be extensively investigated for applications in high power secondary batteries and for their robust stability under large temperature changes. The important material choice factors such as low cost and environmental friendliness make it a suitable cathode material for battery production in the electric vehicle industry [22-24]. Layered $LiNi_xCo_yMn_{1-x-y}$ (NMC) materials are a promising and cost-effective alternative for LIB cathode applications. They can be charged to higher cut-off *voltages* due to the presence of Mn^{4+} which stabilises the structure and provides a higher practically achievable charge capacity (>160 $mAhg^{-1}$). NMC cathode material exhibit high theoretical charge capacity (275 $mAhg^{-1}$) and minimal phase transitions during charge-discharge cycles in the 2.5-4.4 V voltage range. Ni, Mn and Co improve the performance of the NMC cathode material in different ways. Ni-saturated materials exhibit high discharge capacity, Mn provides high cycling life and thermal safety, while Co-saturated materials provide efficient rate capability [67].

2.4. Electrolyte

The function of the electrolyte in a lithium-ion battery is to transport ions between cathode and anode. The electrolyte can be considered as the inert component of the LIB and must show stability against both the cathode and anode surfaces. The electrolyte remains chemically stable during the operation of the LIB and all faradaic processes take place at the electrodes. The electrolyte shall meet the following minimum criteria: (1) a good ion conductor and electron insulator so that lithium ion (Li^+) transport is easy and battery self-discharge is minimal; (2) stable over a wide voltage range, remaining stable over a range of cathode and anode action potentials; (3) inert to other LIB components such as separator, electrode substrate and battery case materials; (4) thermally stable (for liquid electrolytes, both melting and boiling points must be outside the operating temperatures); (5) low toxicity; (6) based on sustainable chemistry, which means that the elements must be available and the synthesis process economic and simple; (7) as low as possible material and production costs. Electrolytes can be divided into: (1) non-aqueous electrolytes consisting of a lithium salt dissolved in an organic solvent or a mixture of solvents, (2) aqueous solutions consisting of a lithium salt dissolved in water, (3) ionic liquids consisting of an organic salt ($R^+ X^-$) doped with a lithium salt equivalent moiety ($Li^+ X^-$), (4) polymer electrolytes - gel polymer and solid polymer, and (5) hybrid electrolytes [68].

2.5. Materials

Fe_2O_3 , which has a high theoretical charge capacity (1006 mAh/g), TiO_2 - which has high cycling stability and reduced graphene oxide (rGO) as an electron conducting filler in poorly conductive transition metal oxide matrices were used for electrode synthesis. Each of these materials has its own lithium storage mechanism. The typical TiO_2 intercalation equation is: $xLi^+ + TiO_2 + xe^- \leftrightarrow Li_x TiO_2$ ($0 \leq x \leq 1$). Titanium dioxide is environmentally friendly, economically viable and characterised by a small change in crystalline lattice volume ($\approx 4\%$) during electrochemical cycling. The major limitations of TiO_2 in battery applications are its low theoretical charge capacity (335 $mAhg^{-1}$) and its poor electrical conductivity, which is in the range of 10^{-12} to 10^{-7} Scm^{-1} [25].

Among transition metal oxides, iron oxide has one of the highest theoretical charge capacities. Fe_2O_3. The most common phases of the material are alpha (hematite), beta, gamma (maghemite), it belongs to group III transition metals. The valence electrons in the iron atom, like all transition metals, are arranged in several orbitals, so that in compounds iron can change its oxidation state, the most common being +2 and +3. As Fe_2O_3 is a widespread naturally occurring, non-toxic, easy to obtain chemical element, it has become a promising material for lithium-ion battery electrode material applications. The storage of lithium is a conversion-type reaction in which iron oxide is reduced to Fe nanoclusters

dispersed in a Li_2O matrix during the insertion of lithium ions, while the delithiation of the electrode material results in a reversible recovery of the elements to their original oxidation states (**see Fig. 2.2**). The reduction and oxidation reactions taking place are: $Fe_2O_3 + xLi^+ + xe^- \rightarrow Li_x Fe_2O_3$ and $Li_xFe_2O_3 + (6\text{-}x)Li^+ + (6\text{-}x)e^- \leftrightarrow 2Fe^0 + 3Li_2O$. Iron(III) oxide binds lithium ions in an electrochemically induced conversion reaction, and 1 mole of iron oxide absorbs 6 moles of lithium $Fe_2O_3 + 6Li \leftrightarrow 2Fe + 3Li_2O$ [26].

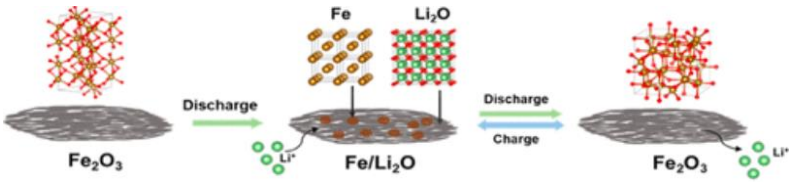

Figure 2.2. Schematic picture of the lithiation-delithiation process of iron(III) oxide electrode material [26].

Graphene is a monolayer of carbon atoms with unique electrical and mechanical properties. Since the synthesis of pure graphene is not economically viable, graphene oxide is used, which is reduced to bring its physical properties closer to graphene. In this study, thermally reduced graphene oxide is used as a conductive additive, from which =O and - OH groups are removed during reduction process [27].

2.6. Technique for fabricating nanocrystalline thin films

The DC electrophoretic material deposition (EPD) method, a simple and cost-effective method requiring only a DC power supply and two conductive substrates placed in suspension, was used to produce the thin films on stainless steel substrates (**see Fig. 2.3**).

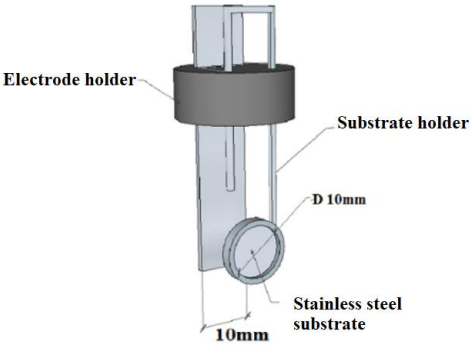

Figure 2.3. Two-electrode system designed for electrophoretic deposition.

During electrophoretic deposition, charged particles in suspension migrate to one of the electrodes under the influence of an external electric field and deposit on it, forming a thin film of precipitate. In this work, the production of a composite material of three substances, Fe_2O_3 , TiO_2 and graphene oxide, by electrodeposition was studied. At the beginning of the work, the experimental boundary conditions

were defined - dispersed phase concentration, electric field value, suspension pH, zeta potential of the suspended particles and deposition time. One of the major advantages of the EPD method is its repeatability and controllability. EPD does not use toxic substances or generate hazardous waste and does not require the addition of binders. During the EPD process it is possible to control the thickness and morphology of the resulting material layer by varying the external electric field and the deposition time.

3. EXPERIMENTAL METHODS

3.1. Preparation of the material

In order to study the use of transition metal oxides and the electrically conductive additive reduced graphene oxides in lithium-ion batteries, it is necessary to prepare the working electrodes or thin films of these materials. To prepare a TiO_2/graphene oxide (GO) suspension, a 22.5 mg TiO_2 nanoparticle powder (Sigma-Aldrich purity ≥99.5%, particle size up to 21 nm) was used and added to 97.5 ml deionised water (DI) previously placed on a magnetic stirrer. Then 2.5 ml of a commercial aqueous GO suspension (BGT Materials, graphene oxide flake size ranging from 1 to 20 µm, suspension pH 7, GO concentration 1 mg/ml) was added. An iron oxide/graphene oxide suspension (Fe_2O_3, Sigma-Aldrich purity ≥99.5%, particle size up to 50 nm) was similarly prepared. To ensure uniform dispersion of the particles in water, the prepared suspensions were aged for one hour in an ultrasonic bath (Amsonic-Branson Ultrasonic cleaning tank, BC series) and then stirred on a magnetic stirrer (t=30 min, V=250 rpm). In order to analyse the physical and electrochemical parameters of pure graphene oxide, the aqueous suspension of pure graphene oxide mentioned above was used for electrophoretic deposition. The electrophoretic deposition was carried out at room temperature (T=293 K), in gavanostatic (constant current) mode, using a DC power supply (*Agilent Technologies N5772A*); the pH of the suspension was measured to be 4 (*pH-meter, Metrohm*), deposition time t = 300 s, electric current I = 31 mA.

To obtain the electrically conductive additive - reduced graphene oxide and to crystallise thin films, the samples were heated in Ar/H flow using a programmable tubular muffle furnace *SNOL 0.2/1250*, heating step 5°C/min. The thicknesses and masses of the obtained films were determined. The thickness was determined using a profilometer (*Veeco Dektak stylus profilometer 150*, needle diameter 12.5 µm). The mass was determined as the difference in mass between the steel substrate before and after the EPD process. A *Mettler Toledo XS105* analytical balance was used for mass determination, maximum mass limit 41 g, accuracy ± 0.01 mg.

To obtain electrode materials for further studies, suspensions were prepared with different molar ratios of Fe_2O_3 and TiO_2 - 1:1, 2:1 and 3:1. The term 'molar ratios' will be used in the context of this work to refer to the process of preparing the suspensions, where the molar masses of each chemical compound are taken into account when weighing the materials. The electrode materials were labelled FT11, FT21 and FT31, containing the first letter of the Latin name of each transition metal oxide and the molar mass fraction of the material used in the suspension preparation. 10 wt% graphene oxide was used as a conductive additive, which is reduced after nanocomposite thin films were obtained.

3.2. Studies on the composition, structure and morphology

Scanning electron microscopy was performed using a microscope *(SEM, Tescan Lyra 3*, electron accelerating voltage 5 - 15 kV) to evaluate surface morphology, particle size and homogeneity of the thin films. For X-ray diffraction (XRD) measurements a *Rigaku MiniFlex 600* diffractometer was used, with Cu anode, diffraction angle accuracy ±0.02°, used X-ray wavelength CuK_α = 1.54 Å, operating voltage 45 kV, current 40 mA. In order to verify the successful reduction of graphene oxide to rGO, Raman spectroscopy was performed using a Raman spectrometer *TriVista CRS Confocal TR777*, manufacturer "*GmbH*", wavenumber range 10 cm^{-1} - 9000 cm^{-1} , resolution 0.1 cm^{-1} , laser wavelength used 532 nm. In order to assess the active surface area and porosity of the obtained material films, BET *(Brunauer-Emmett-Teller)* analysis was performed using nitrogen sorption processes on solid particles (*NOVA series, High speed surface area & Pore Size analyser*, Latvian Institute of Wood Chemistry). In order to assess the relief of the obtained thin films, the surface was analysed by Atomic Force Microscopy (*AFM, Renishaw*) in the touch-up mode (Si needle, r = 10 nm). X-ray microspectral analysis (*EDX*) was performed using a (*SEM, Tescan Lyra 3,* electron accelerating voltage 5- 15 kV, detector

EDX Oxford X-Max 50 mm^2) to obtain information on the composition of the nanocomposite films and to estimate the amount of chemical elements. X-ray photoelectron spectroscopy (*XPS*) was performed to determine the valence and the amount of chemical elements present on the surface of nanocomposite material films using a instrument *(ESCALAB Xi, "ThermoFisher")*. XPS spectra were taken in a vacuum chamber at pressures below $2\text{-}10^{-10}$ Torr using Al K_α X-rays with energy ≈1.5 keV.

3.3. Electrochemical measurements

The electrochemical performance of electrode materials was measured by assembling battery *half-cells*. Obtained films were used as the working electrode and lithium metal as the counter electrode (reference electrode). The whole system is contained in the electrolyte, with a separator separating the working electrode and the lithium metal. It should be noted that the complete cell consists of a battery cell with both cathode and anode material as electrodes. The performance of the Fe_2O_3/rGO, TiO_2 /rGO and rGO electrode materials were carried out in a *Swagelok* type cell, material 316 stainless steel, inner diameter 12.7 mm. The battery half-cells were assembled in an argon-filled glove box (*Glove Box*, *Unilab Pro Eco 4 gloves*, manufacturer *MBraun*, O_2 0.5 ppm, H_2O 0.5 ppm) using a commercial electrolyte $LiPF_6$ 1M solution in ethylene carbonate (EC) and dimethyl carbonate (DMC), solvent weight ratio 1:1 (*Sigma-Aldrich*, purity ≥98.0%). A *Proline Plus* micropipette *(Sartorius) (*20-200 μL, ±0.02 μL) was used for accurate electrolyte volume measurement. The separator was a *Whatman* glass microfibre filter GF/F (average pore diameter 0.7 μm) and the reference electrode was lithium metal (*Sigma Aldrich,* 0.75 mm x 19 mm). A 5 wt% fluoroethylene carbonate (FEC) additive was used to ensure the formation of a stable, homogeneous solid – electrolyte interface. Battery measurements (rate capability, cyclability, cyclic voltammetry - CV and electrochemical impedance spectroscopy - EIS) were performed by potentiostat-galvanostat *BioLogic VMP3.* Impedance equivalent circuit results were obtained and analysed using *EC-Lab V11.41, Z-FIT-Bio-Logic* software.

4. RESULTS AND DISCUSSION

4.1. Study of electrophoretically deposited iron oxide, titanium dioxide and reduced graphene oxide as electrode material

The masses of Fe_2O_3/rGO, TiO_2/rGO and rGO films were estimated to range from 0.35 - 0.65 ± 0.01 mg, while the thicknesses ranged from 2.2 - 4.8 ± 0.1 μm. Scanning electron microscopy (SEM) analysis shows Fe_2O_3 and TiO_2 nanoparticles and agglomerates embedded in the rGO layers and bound to its surface (**see Figure 4.1**). The grain size of the titanium dioxide detected ranges from 30-50 nm. Iron oxide grain size 300-500 nm.

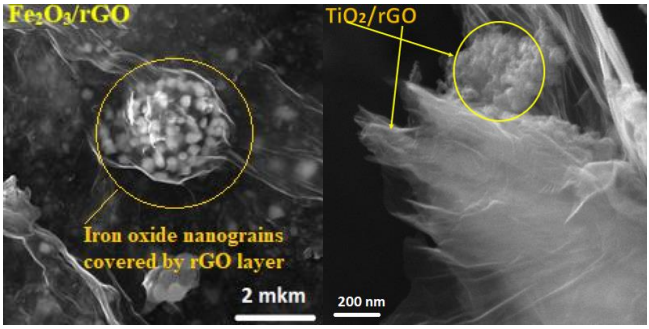

Figure 4.1. SEM images of Fe_2O_3/rGO and TiO_2/rGO layers.

X-ray diffraction (XRD) analysis reveal the films consist of iron oxide γ- Fe_2O_3 (maghemite), anatase phase TiO_2 and a small admixture of rutile phase TiO_2. The presence of rGO has been identified in TiO_2/rGO sample. The calculated average crystallite size is 19.5 nm for Fe_2O_3/rGO and 42.8 nm for TiO_2/rGO. Analysis of Raman spectra revealed presence of reduced graphene oxide in the nanocomposites and the intensity of G-band located at a wavenumber value 1600 cm^{-1} is slightly higher than the D-band intensity at 1350 cm^{-1}. It is also confirmed by decrease of I_D/I_G band intensity ratio value. For graphene oxide calculated value of I_D/I_G is 1.1, while after its reduction I/I_{DG} = 0.96 respectively, which shows that the ratio of D and G band intensities has decreased by 13% during reduction process. The reduction process of graphene oxide has been successful and a partial recovery of the carbon atomic structure has occurred. A broad peak in the wavenumber range from 2500 to 3500 cm^{-1} indicates presence of few layered graphene *(FLG)* [28-30]. The BET analysis showed that the TiO_2 /rGO material has largest surface area 50.2 ± 0.1 m^2g^{-1} and pore volume 0.16 ± 0.05 cm^3g^{-1}, both measured values being close to the results reported in scientific literature. The average pore diameter for both transition metal oxide films was found to be approximately 12 nm [31]. It should be noted that Fe_2O_3/rGO and TiO_2/rGO showed higher values of pore volume and average pore diameter compared to the pure reduced graphene oxide thin film.

Rate capability tests of obtained electrode materials were performed and applied current increased from 0.5C to 2C, gravimetric capacities of the Fe_2O_3/rGO, TiO_2 /rGO and rGO decreased by 64%, 73% and 77%, respectively. The result indicates that Fe_2O_3/rGO shows the highest tolerance to current increase. Galvanostatic profiles were constructed to identify possible plateaus at certain voltage values and to characterise the charge-discharge curves of the electrode materials (**see Fig. 4.2).**

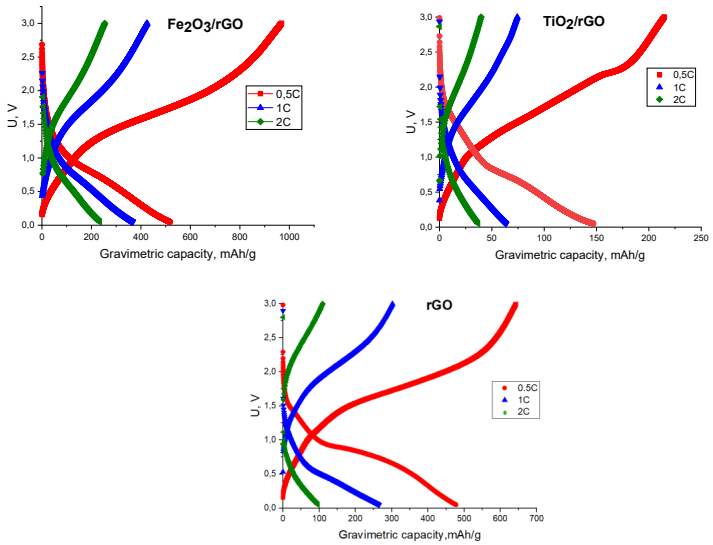

Figure 4.2. Galvanostatic profiles of Fe_2O_3/rGO, TiO_2 /rGO and rGO electrode materials.

The galvanostatic charge-discharge curves did not show any distinct charge-discharge plateaus characterising the electrochemical performance of the materials. The electrode material Fe_2O_3/rGO at a current 0.5 C showed a small discharge plateau at 0.8 V, characteristic of a gradual reduction process of Fe_2O_3 from Fe^{3+} to Fe^0. For TiO_2/rGO and rGO electrode materials, an unresolved plateau in the voltage range of 0.6 - 0.9 V was found, consistent with the intercalation of the lithium into the material structure [32-33]. The highest gravimetric capacitances of the electrode materials were determined at a discharge current 0.5 C for Fe_2O_3/rGO = 604 $mAhg^{-1}$, TiO_2/rGO = 280 $mAhg^{-1}$ and rGO = 473 $mAhg^{-1}$. Cyclability performance revealed that the TiO_2/rGO electrode material (**see Fig. 4.3**) exhibited the highest cycling stability, as characterised by the percentage of charge capacity retained after cycling, wich gives possibility to use TiO_2 as a stabilising matrix to improve other possible LIB electrode materials with lower cyclability characteristics but higher theoretical capacity.

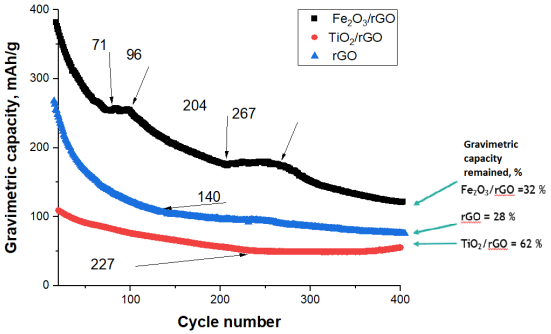

Figure 4.3. Charge capacity as a function of the number of discharge cycles.

The aim of this work is to study transition metal oxide as LIB electrode materials, and rGO is used as an electron conducting additive to poorly conducting Fe_2O_3 and TiO_2 matrices, the electrochemical activity of rGO is not further considered. Cyclic voltammetry (CV) measurements of Fe_2O_3/rGO, TiO_2/rGO electrode materials (**see Figure 4.4**) revealed characteristic lithium injection and extraction peaks for Fe_2O_3 and TiO_2 and high reversibility of the redox reactions as evidenced by the overlap of several CV cycles.

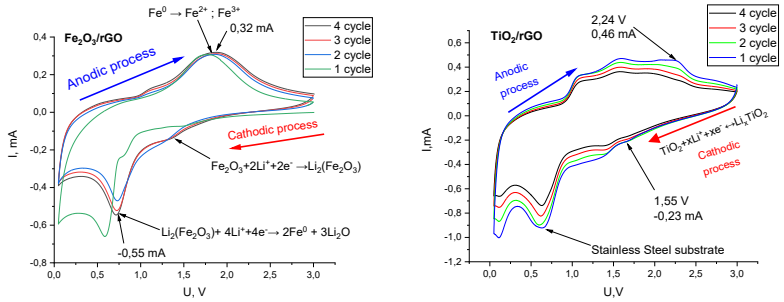

Figure 4.4. CV curves of the first four cycles of Fe_2O_3/rGO and TiO_2/rGO. Voltage sweep rate 1 mVs^{-1}, voltage range 0.05-3 V.

For the Fe_2O_3/rGO electrode material, an increase of current flowing through the electrode with increasing number of charge-discharge cycles is observed, which agrees with the results obtained by electrochemical impedance spectroscopy. The possible causes of the observed phenomenon are: the formation of metal nanoparticles during the successive charge-discharge of transition metal oxides, which improves the electrical conductivity of the electrode [34], and electrochemical cycling improves the interactions between nanoparticles in the nanocomposite, which enhance its electrical conductivity and lithium ion kinetics [35]. The lithium injection current values of TiO_2/rGO electrode materials decrease slightly during multiple CV cycles, which indicate electrode polarisation and growth of SEI (*solid - electrolyte interface*) layer [36]. Using the Randles-Sevchick equation [2-3], the chemical diffusion coefficients of cathodic cycle lithium were calculated: $D(Fe_2O_3/rGO) = 16 \cdot 10^{-14}$ cm^2/s and $D(TiO_2/rGO) = 1 \cdot 10^{-14}$ cm^2/s. Comparison of cyclic voltammetry curves for studied electrodes with the charge-discharge profiles showed that the voltage values of the cathodic lithium injection peaks have some approximation to the identified discharge plateau regions in the charge-discharge profiles (**see Fig. 4.2**). A good agreement between the experimental and calculated spectra was observed when analysing the results obtained using electrochemical impedance spectroscopy (EIS). The determined charge transfer resistance (R_{ct}) for the TiO_2/rGO electrode is 15 Ω/cm^2 ,which is significantly lower than for Fe_2O_3/rGO electrode (R_{ct} = 131 Ω/cm^2). This result demonstrates a strategy how to facilitate charge transfer, e.g. by integrating both transition metal oxides in a single electrode material. The results of the equivalent circuit modelling of the EIS spectra, plots of charge transfer resistance and Warburg impedance as a function of battery half-cell voltage were constructed (**see Fig. 4.5**).

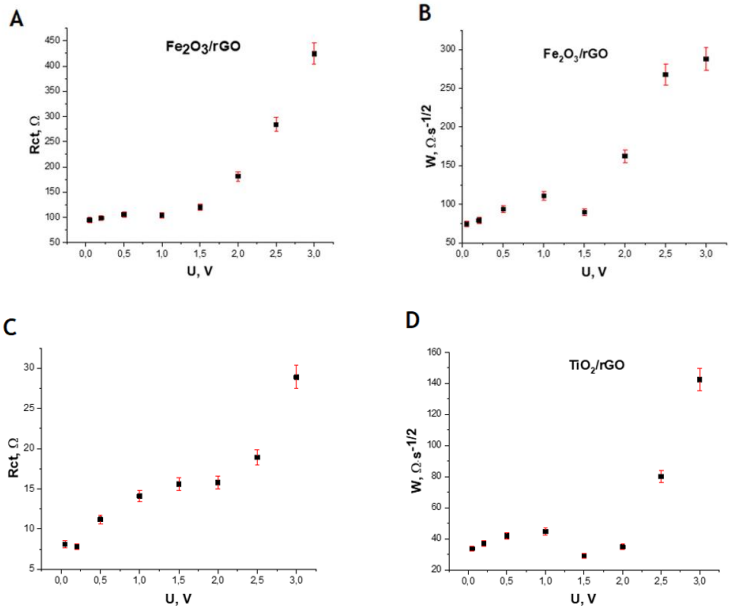

Figure 4.5. Fe_2O_3/rGO and TiO_2/rGO electrode material charge transfer resistance (A, C) and Warburg impedance (B, D) as a function of battery half-cell voltage.

It was found that the more the battery half-cell is discharged and electrode is saturated with lithium ions, more charge transfer (R_{ct}) and lithium diffusion resistance decrease. The observed exponential relationship eventually leads to possibility of developing a method in which the state of charge of LIB would be evaluated on the basis of R_{ct} and the value of Varburg impedance. The Varburg impedance of Fe_2O_3/rGO and TiO_2/rGO electrode materials increases (**see Fig. 4.5 B, D**) with increasing battery half-cell voltage. The calculated lithium diffusion coefficients decrease with increasing voltage as they are inversely proportional to the Varburg impedance values. The maximum values of the Warburg impedance correlate with the minimum of diffusion coefficient. The diffusion coefficient of lithium determined by EIS shows values of $D(Fe_2O_3/rGO)=1\cdot10^{-16}$ cm^2/s, and $D(TiO_2/rGO)=5\cdot10^{-16}$ cm^2/s [37-38]. The diffusion coefficient values for lithium determined by CV and EIS differ by several orders of magnitude, the reason is still under investigation, but difference in diffusion coefficients determined by two methods has also been observed by other authors [39].

4.2. Studies of different quantitative compositions iron oxide and titanium dioxide electrode materials

Using analytical balance and surface profilometry, the masses and thicknesses of the FT11, FT21 and FT31 nanocomposite thin films were determined, ranging from 0.55 - 0.93 ± 0.01 mg and 3.8 - 6.1 ± 0.1 μm, respectively. Analysis of the SEM images showed a Fe_2O_3 and TiO_2 nanoparticles and their agglomerates anchored on reduced graphene oxide matrix **(see Figure 4.6 A)**. A separate rGO flake was found on the surface of nanocomposite, coated with Fe_2O_3 and TiO_2 nanoparticles (**see Fig. 4.6 B**). This indicates the high adhesivity of the nanoparticles. The reduced graphene oxide flakes in nanocomposite material structure act as a stabiliser, either by binding nanoparticles to the surface or by incorporating them into layered structure of rGO. The resulting material is mechanically stable and ensures the preservation of Fe_2O_3 crystalline structure during electrochemical cycling [40].

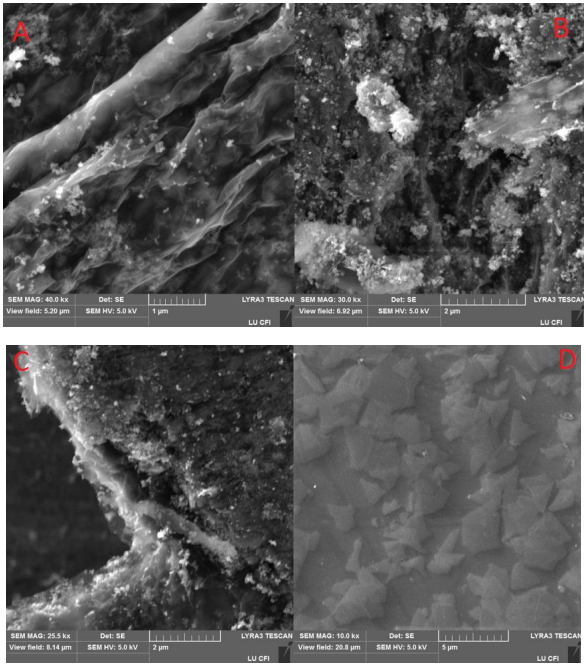

Figure 4.6. Scanning electron microscopy images of A - FT11, B - FT21, C - FT31 and D - graphene oxide flakes .

Further analysis of the SEM images revealed that the deposition of graphene oxide flakes produces multilayer graphene oxide material (**see Figure 4.6 C**), which is also confirmed by the Raman spectroscopy results. The average dimensions of the graphene oxide flakes are 3114 μm (length) and 1554 μm (width), (**see Figure 4.6 D**). The films were assessed to be inhomogeneous and granular, and particle agglomerates were detected, also confirmed by atomic force microscopy. Summarising the observations, it is concluded that electrophoretic deposition produces a thin layer of material deposited on the steel substrate consisting of both individual Fe_2O_3 and TiO_2 nanoparticles and their agglomerates. The average particle diameters determined for FT11, FT21 and FT31 were found to be similar in the range 98-120 nm, however, a slight trend of increasing size with increasing amount of Fe_2O_3 in nanocomposite was observed.

The active surface area and porosity of thin films were evaluated and it was found that the active surface area and pore volume decrease with with increasing amount of Fe_2O_3. The average pore diameter of the nanocomposite thin films is ≈ 12.5 nm. In order to assess the relief of the FT11, FT21 and FT31 nanocomposite thin films, the surface was observed (**see Figure 4.7**) using atomic force microscopy.

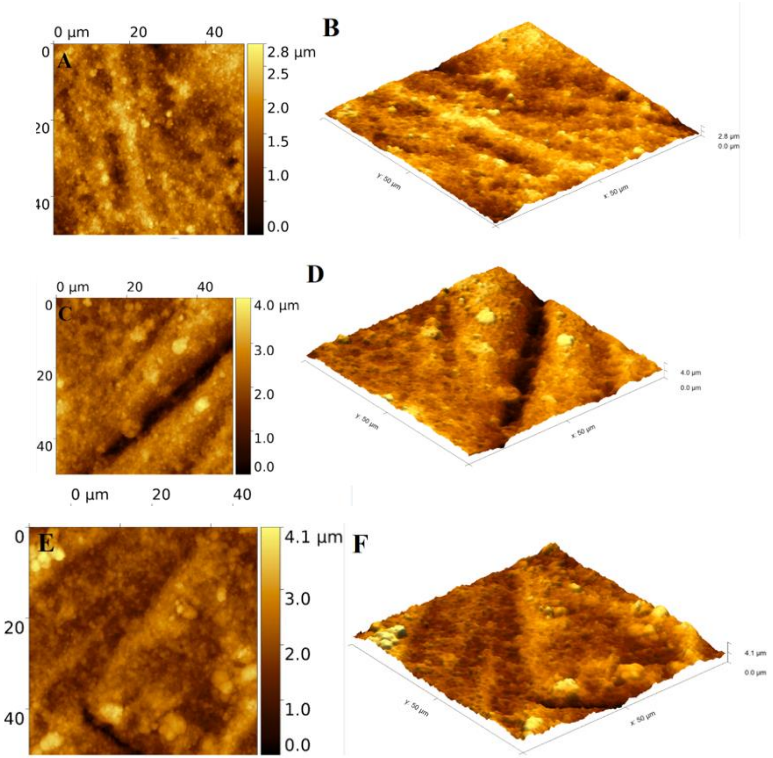

Figure 4.7. Results of Atomic force microscopy. A, B - FT11, C, D - FT21, E, F - FT31.

Agglomerates of Fe_2O_3 and TiO_2 nanoparticles, diameters in the range of 2-3 µm, were observed for the nanocomposite (**see Figure 4.7 B, D, F**), consistent with the results obtained by SEM. Relief changes, mainly depressions and elevations, were observed between the grains, but no cracks were detected, indicating the stability of the film during heating process. Within a single agglomerate, the height variation ranges from 1-3 µm. Summarising the results, it was concluded that the relief significantly increases the actual surface area and all samples have agglomerates on the its surface.

Analysis of the X-ray diffraction patterns showed that the nanocomposite thin films consisted of a maghemite phase Fe_2O_3 (denoted by F) and an anatase phase TiO_2 (denoted by T) with a small admixture of a rutile phase TiO_2 [164], demonstrating that, for the first time, composite layers of Fe_2O_3 and TiO_2 were successfully obtained by DC electrophoretic deposition. In order to study whether the nanocomposite thin films contained different amounts of Fe_2O_3, a graph was constructed plotting the numerical value of each characteristic iron oxide peak intensity as a function of the X-ray diffraction angle [41-42] (**see Fig. 4.8**).

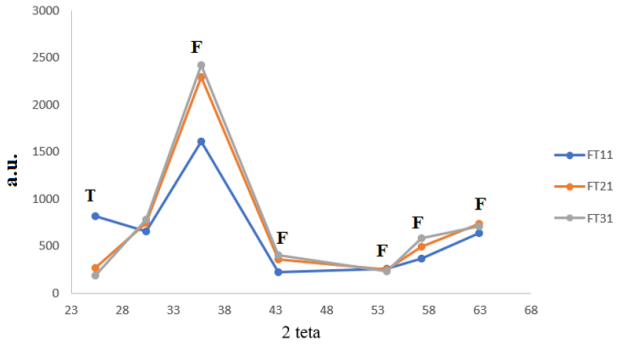

Figure 4.8. Comparison of X-ray diffractogram intensities of FT11, FT21 and FT31 nanocomposites .

Using an open source program (*Profex BGMN 5.2.0*), the amount of material phases was estimated using the Rietveld method (**see Table 4.1**). The analysis revealed that nanocomposites FT21 and FT31 correspond to the molar ratios of materials defined during suspension preparation for electrophoretic deposition. A slight deviation from the original amount was found for nanocomposite FT11, where the calculated weight percentage was 55:45 wt.%, although the weight percentage ratio prepared in suspension was 60:30 wt.%. The deviation from the initial set-up found in FT11 nanocomposite layer suggests that suspensions containing elevated concentrations of TiO_2 nanoparticles undergo a faster deposition process, increasing the amount of TiO_2 in the deposited layer.

Summarising the Raman spectroscopy results, it is concluded that the reduction process of graphene oxide was successful and the crystallisation of reduced graphene oxide increased, as confirmed by calculated rGO crystallite dimensions. The ratio of intensities for I_D and I_G bands, which characterises the presence of carbon defects and ordered structure, decreased by 8% after graphene oxide reduction, confirming the success of reduction process [43].

X-ray microspectral analysis (*EDX*) and X-ray photoelectron spectroscopy (*XPS*) were performed to obtain information about composition of nanocomposite and to estimate the amount of chemical elements. Summarising the results, it was found that the nanocomposite materials consist of Fe, Ti and O, which are present also in certain materials used to prepare the initial suspension. Quantitative analysis showed a gradual increase of Fe with increasing amounts in the prepared suspensions.

It was found that with the increase concentration of Fe_2O_3 nanoparticles in the suspension, the amount of TiO_2 nanoparticles deposited by EPD also increased. The analysis of EDX spectra showed that the measured positions of the Fe intensity peaks on the x-axis correspond to the maghemite phase of iron oxide [44], while the Ti peaks correspond to the anatase phase of titanium dioxide [46]. The distribution of Fe, Ti and O is relatively homogeneous, confirming the uniform deposition of particles during EPD [45]. In the nanocomposite FT31, several regions of increased Ti concentration were found, which could indicate increased agglomeration of TiO_2 nanoparticles in the prepared suspension or during electrodeposition. The presence of these agglomerates in the precipitated layer explains the increased Ti content in the FT31 nanocomposite material.

Analysis of the XPS spectra revealed typical peaks at the energy levels of Fe, Ti, C and O atoms. The x axis values of the measured XPS peaks are similar for the materials, but the characteristic areas under the curve are different. Based on the above, it is concluded that the nanocomposite are composed of the same chemical elements, the amount of which varies from composite to composite. The quantitative analysis of the chemical elements showed a gradual increase of Fe and a decrease of Ti in the in proportion to the composition of prepared suspensions. The highest value of titanium weight percentage was observed for nanocomposite FT11, which is in agreement with the calculation of the Rietveld method used in X-ray diffraction analysis. Comparison of the quantitative calculations performed by XPS, EDX and XRD showed that all methods used to study materials showed an increase

of Fe content with increasing molar fraction of iron in suspension (**see table 4.1**). This observation leads to conclusion that the EPD method can be applied to customize the composition of the material by preparing suspensions with specific molar ratios of the materials

Table 4.1. Quantitative estimation of the FT11, FT21, FT31 nanocomposites

Nano-composite material	Average crystallite size, nm	Chemical element content determined by EDX, wt%			Chemical element content determined by XPS, wt%				Quantities of material phases calculated from XRD data by the Rietveld method, wt%		
		Fe	Ti	O	Fe	Ti	O	C	Fe_2O_3 (maghemit phase)	TiO_2 (anatase phase)	TiO_2 (rutile phase)
FT11	37 ± 2	67	4	29	62	30	6	2	55±0.01	35±0.01	10±0.01
FT21	24 ± 2	72	5	23	71	23	3	3	79±0.02	14±0.01	7±0.02
FT31	32 ± 2	76	7	17	80	13	2	5	88±0.02	9±0.01	3±0.01

To evaluate the application of FT11, FT21 and FT31 nanocomposite materials in lithium-ion batteries, battery half-cells were assembled and electrochemical performance measurements were performed. Galvanostatic analysis of the charge-discharge curves (**see Figure 4.9**) showed that among the electrode materials, the FT31 nanocomposite has the highest gravimetric capacity 729 mAh/g or 68 % of theoretical charge capacity, which is 17 % higher than the charge capacity of Fe_2O_3/rGO (604 $mAhg^{-1}$). Some research groups report improved gravimetric capacitance of Fe_2O_3 and TiO_2 composite electrode compared to pure transition metal oxide electrode materials, suggesting that electrochemical activity of Fe_2O_3 and TiO_2 nanoparticles effectively interact and create an electrode material with higher gravimetric capacitance [47-51].

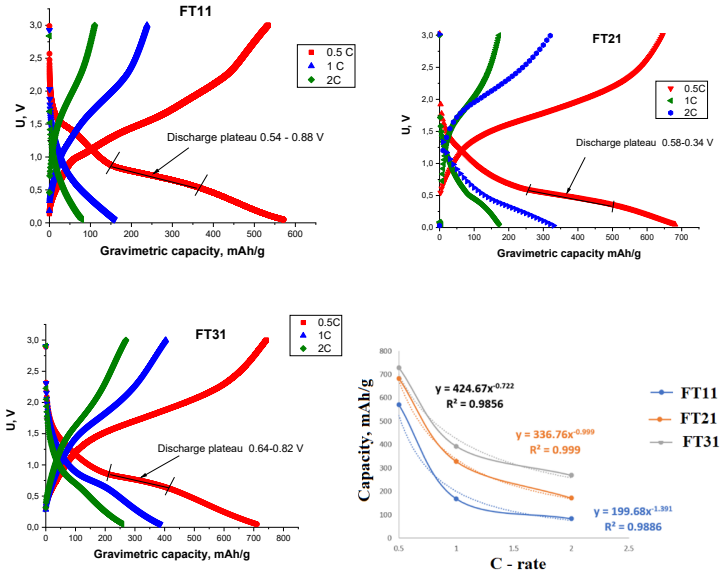

Figure 4.9. Galvanostatic charge-discharge curves of FT11, FT21 and FT31 nanocomposite electrodes taken at current strengths of 0.5C, 1C and 2C and charge capacity as a function of discharge current.

At a current value 0.5C, the charge - discharge curves show small, quasi-linear regions in the voltage range 0.4 to 0.8 V, corresponding to a gradual reduction process of Fe_2O_3 and Fe^{3+} changes oxidation state to Fe^0. In this reaction, an electrode-electrolyte interface (SEI) layer and Li_2O are formed [47]. The gravimetric capacities of nanocomposite electrode materials FT11 and FT21 are 571 mAh/g and 683 mAh/g, or 77 % and 88 % of the theoretical gravimetric capacity, respectively.

The FT21 nanocomposite electrode material exhibited a gravimetric capacity value closest to its theoretical gravimetric capacity. From this observation, it can be concluded that the FT21 electrode material is characterised by the highest lithium injection and electrochemical activity. The rate capability tests on FT11, FT21 and FT31 electrode materials show the gravimetric capacity decreases gradually with increasing current. For example, as the value of applied current increased from 0.5C to 2C, the respective gravimetric charge capacities of the electrode materials FT11, FT21 and FT31 decreased by 85 %, 77 % and 64 %. Among all electrode materials, the FT31 nanocomposite has the highest tolerance against current increment.

In order to assess the ability of electrode materials to maintain their gravimetric capacity over multiple charge - discharge cycles, a plot of capacity as a function of the number of cycles was constructed (**see Figure 4.10**).

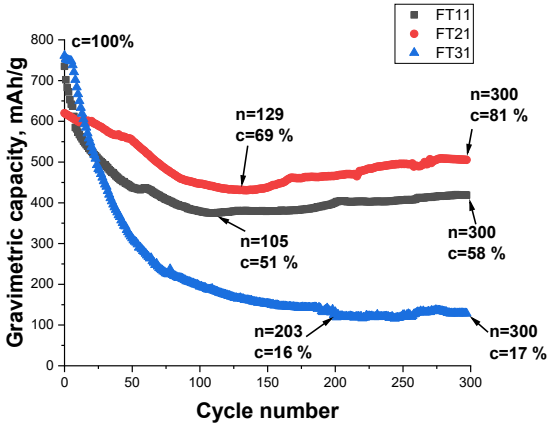

Figure 4.10. Gravimetric capacity of FT11, FT21 and FT31 as a function of the number of cycles.

From constructed curves it is clearly seen that all electrode materials show a gradual capacity decrease during the initial charge-discharge cycles, which is due pulverisation of iron oxide particles during lithium injection-extraction, causing a loss of electrical contact between the electrode material and current collector. Pulverisation is the loss of homogeneous structure of electrode material due to tension and/or compression, caused by repeated change in particle volume during the lithium injection and extraction process [66]. Comparison of cyclability curves showed that the slowest decrease of capacity during cycles was for FT11 and FT21 electrode materials. The improved electrochemical performance is probably due to the increased amount of TiO_2 in the electrode material. (**see Table 4.1**) The titanium dioxide nanoparticles inhibit the pulverisation of the Fe_2O_3 particles while maintaining their structural integrity, which can be observed as a curves slope stabilisation for FT11 and FT21 after hundred charge-discharge cycles. The highest retention of charge capacity is observed for the nanocomposite electrode material FT21, which retains 69 % of its initial gravimetric capacity value after 129 charge-discharge cycles. As the cycling process continues, the gravimetric capacity of FT21 increases and reaches a value of 508 mAh/g or 81 % of the initial charge capacity. The increase of capacity during electrochemical cycling process is not characteristic of nano-sized Fe_2O_3 composites but was also observed for other conversion-type 3D transition metal oxides such as Co_2O_3 and MnO_2 [52]. Several mechanisms were put forward to explain the increase of capacity:

1) In low voltage range 0-1.9 V, as the electrolyte is reduced, an organic polymer-gel film is formed around the metal nanoparticles, into which lithium ions are incorporated, providing an additional charge capacity up to 800 charge-discharge cycles [53-54],

2) uncompensated lithium ions accumulate in the interfacial space between the metal nanoparticles and electrolyte, compensated by electrons from the nanoparticle surface [55-57],

3) new lithium injection "sites" are formed in the electrode material during cycling, i.e., resulting in additional charge capacity of the electrode material [6; 58],

4) Fe nanoparticles, formed as a side product of irreversible reactions and localised at the grain boundary surface of Fe_2O_3/TiO_2, hence improve the electrical conductivity of active material and facilitate the oxidation - reduction reactions,which finally provides additional capacity [6; 59-61].

The additional gravimetric capacity observed for FT11 and FT21 is probably related to the reactions occurring on the surface of material. Surface charge storage is divided into faradaic (pseudocapacitance) and nonfaradaic (electric double layer capacitance). The pseudocapacitive charge storage mechanism is more relevant for charge storage in SEI layer and at the metal nanoparticle/Li_2O interface. The electric double layer energy storage mechanism refers to the static storage of electric

charge for materials with large surface area [62].

Cyclic voltammetry (CV) was performed to obtain information about lithium ion injection-extraction peaks, electrochemical activity of FT11, FT21 and FT31 electrode materials and data acquisition for lithium ion diffusion coefficient calculations (**see Figure 4.11).**

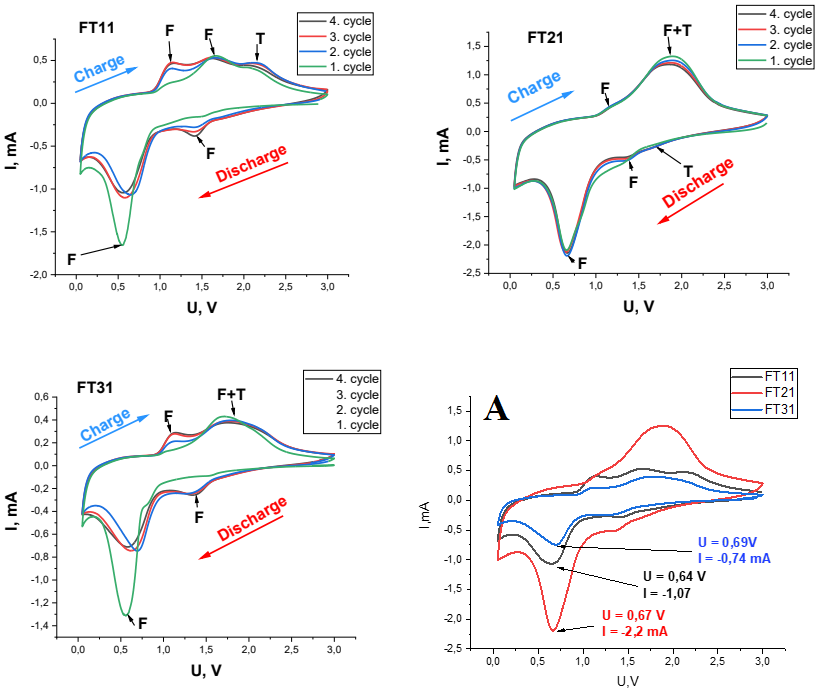

Figure 4.11. Cyclic voltammograms of FT11, FT21 and FT31 nanocomposite electrodes at a voltage step rate 1 mVs^{-1}. Characteristic current peaks denoted as F – Fe_2O_3 and T - TiO_2 materials. Picture A - first cycle of FT11, FT21 and FT31.

It was found that for nanocomposites FT11 and FT31 in the discharge cycle, the intensity of cathodic current peak at voltage value ≈ 0.6 V is highest in the first cycle. In following cycles, the intensity of current peak decreases, which indicates irreversible chemical reactions in the electrode material and a partial loss of initial capacity, which takes place during the electrochemical stabilisation of electrode and related to SEI layer formation [64-65]. The FT21 electrode material exhibit highest lithium injection current peak (I=2.2 mA) (**see Figure 4.11 A**) and the best reversibility of reactions, confirming the high electrochemical activity. The data obtained by the CV method were used to calculate lithium diffusion coefficient. Results revealed, that the FT11 and FT21 nanocomposite electrode material shows the highest lithium diffusion coefficients. Summarised the results obtained by cyclability measurements, electrochemical activity evaluation and lithium diffusion coefficient calculation, the FT11 and FT21 nanocomposite electrode materials were chosen for further studies.

The analysis of the results obtained by electrochemical impedance spectroscopy (EIS) showed that the lowest charge transfer resistance (R_{ct}) at battery half-cell voltage U = 0.5 V was observed for the FT21 electrode (R_{ct} =15.4 Ω), which is 40% lower than for the FT11 electrode material. The lower value of R_{ct} indicates an efficient charge transfer and thus a higher rate capability of the FT21 electrode material [212], which is also confirmed by previous FT21 rate capability measurements. For the

nanocomposite electrode FT21, a good agreement of the experimental EIS spectrum with the calculated was observed (**see Figure 4.12**).

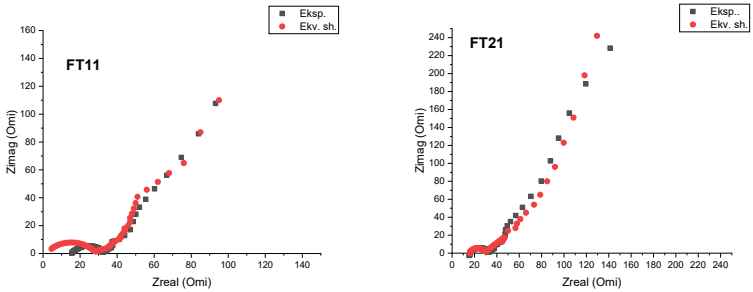

Figure 4.12. Experimental and calculated EIS spectra of FT11 and FT21 electrodes at U = 0.5 V.

To analyse the charge transfer resistance as a function of the battery half-cell charge voltage, plots of R_{ct} =f(U), were constructed (**see Fig. 4.13**).

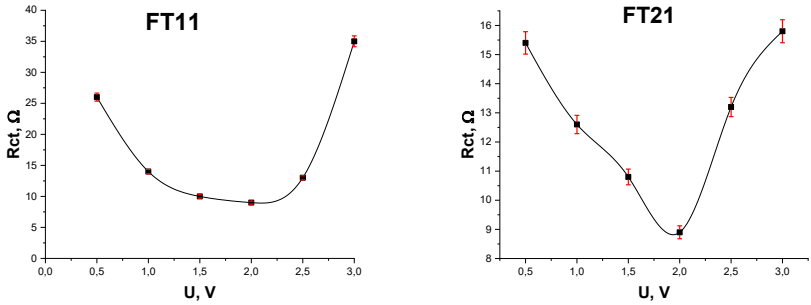

Figure 4.13. Charge transfer resistance as a function of the state of charge of the battery half-cell.

Analysis of R_{ct} = f(U) curve showed a significant dependence of R_{ct} and state of charge of the battery half-cell. The value of charge transfer resistance decreases as the battery half-cell is recharged to about 60% or ≈ 2 V and then increases again, approaching and even exceeding the initial value of R_{ct} at 100% battery half-cell charge. It is worth noting that the voltage value of 2 V is equal to the open circuit potential or equilibrium voltage of battery half-cell. This dependence of charge transfer resistance and state of charge is also in agreement with other authors [63-64]. The lithium diffusion coefficient determined by the EIS shows values D(FT11) = $7 \cdot 10^{-16}$ cm^2/s, and D(FT21) = $9 \cdot 10^{-16}$ cm^2/s. **Table 4.2** was created to compare the calculated diffusion coefficients.

Table 4.2. Lithium diffusion coefficients determined by EIS and CV methods.

	Cyclic voltammetry, D, cm/s^2	Electrochemical impedance spectroscopy, D, $cm^2/s \cdot 10^{-16}$
Fe_2O_3/rGO	$1.6 \cdot 10^{-13}$	1
TiO_2/rGO	$1 \cdot 10^{-14}$	5
FT11	$6 \cdot 10^{-13}$	7
FT21	$1.2 \cdot 10^{-12}$	9

The table shows the lithium diffusion coefficients obtained by both methods are higher for Fe_2O_3 and TiO_2 composite materials, indicating the positive effect of combining the two transition metal oxides to facilitate lithium diffusion in electrode material.

CONCLUSIONS

The aim of the work has been achieved: Fe_2O_3, TiO_2 and reduced graphene oxide composite thin films have been obtained by electrophoretic deposition. Their physical and electrochemical properties depending on the composition of the suspension were studied and the applicability of the electrode material in lithium-ion batteries was assessed. According to the chapters in which the results are discussed, there are 2 main conclusions.

1. The electrophoretic deposition method can successfully produce mechanically stable and porous two-component battery electrode materials from Fe_2O_3, TiO_2 and reduced graphene oxide conductive additive, in which transition metal oxide nanoparticles and agglomerates successfully combine with reduced graphene oxide - Fe_2O_3/rGO and TiO_2/rGO. Despite the high theoretical gravimetric capacity of iron oxide (1006 mAh/g), the value achieved in practice is 604 mAh/g, which leads to the search for new approaches to increase the experimental capacity and improve stability of iron oxide. From the cyclic voltammetry results, the highest lithium diffusion coefficient was determined for the Fe_2O_3/rGO electrode material ($1.6 \cdot 10^{-13}$ cm^2 /s) and it was concluded that the current flowing through the electrode increases with increasing number of cycles. The TiO_2/rGO electrode material showed a rapid decrease in gravimetric capacity with increasing discharge current but high stability in cyclability measurements, which opens the possibility for use TiO_2 to improve the cycling performance of high gravimetric capacity materials.

2. Three-component Fe_2O_3/TiO_2/rGO nanocomposite thin films with different transition metal oxide mass fractions were obtained for the first time by electrophoretic deposition. The mass fraction of iron oxide and titanium dioxide in the obtained thin films was found to be similar to that in the prepared suspensions, as confirmed by X-ray diffraction analysis and Rietveld method. The nanocomposite FT21 have the highest lithium injection current peak and highest lithium diffusion coefficient ($1.2 \cdot 10^{-12}$ cm^2/s) as well as a high reversibility of the oxidation - reduction reaction, due to the high electrochemical activity of material. For nanocomposites FT11 and FT21, an increase of gravimetric capacity was observed during electrochemical cycling, which is related to the faradaic and non-faradaic electric charge storage activity. For example, the gravimetric charge capacity of FT21 increases during cycling from 442 mAh/g to 508 mAh/g which is 81% of the initial capacity. Compared to pure transition metal oxide electrode material, the Fe_2O_3 and TiO_2 nanocomposite has a higher lithium diffusion coefficient, confirming the positive effect of combining two materials to facilitate lithium diffusion. The nanocomposite FT21 electrode material has a gravimetric capacity 683 mAh/g at a discharge current 0.5 C, which is 88% of its theoretically calculated capacity. Based on the results of rate capability, cyclability and capacity measurements, the nanocomposite with 2:1 molar concentrations of Fe_2O_3 and TiO_2 (FT21) is a promising high performance electrode material for lithium - ion batteries.

THESES TO BE DEFENDED

An electron and lithium ion conducting iron(III) oxide/titanium dioxide/graphene oxide thin-film composite material and an environmentally friendly and cost-effective technology for its production have been developed to optimise the anode material for lithium-ion batteries.

- The electrophoretic deposition method can be successfully used to produce Fe_2O_3, TiO_2 and graphene oxide nanocomposite thin films from commercially available materials. The obtained films are porous and mechanically stable without binding agents.

- Two-component Fe_2O_3/reduced graphene oxide (rGO) material as a battery electrode shows higher gravimetric capacity, while titanium dioxide TiO_2/rGO electrode shows higher stability during charge-discharge cycles. High gravimetric capacity of the Fe_2O_3/rGO could be attributed to both a conversion-type reaction of iron oxide lithiation process, a multi-electron process during 6 electrons and 6 lithium ions are transferred per one mole of Fe_2O_3, and a pseudocapacitive charge storage mechanism related to the iron oxide and carbon heterostructures. High stability of titanium dioxide, on the other hand, is due to the similar radii of Li^+ and Ti^{3+} ions, resulting a small (≈ 4 %) changes of TiO_2 crystal structure during the lithium intercalation process, maintain the integrity of material.

- The electrochemical properties of ternary Fe_2O_3/TiO_2/rGO electrode and hence the battery performance can be improved by varying molar concentrations of the Fe_2O_3 and TiO_2 in suspension. Among materials, the best electrode composition was found, with a molar ratio Fe_2O_3 and TiO_2 of 2:1 (FT21), which provides both high gravimetric capacity and stability during the multiple charge-discharge process.

REFERENCES

[1] M. Wakihara, O. Yamamoto, Lithium Ion Batteries, Fundamentals and Performance, WILEY-VCH, ISBN: 978-3-527-61198-0, November 2008, 261 Pages.

[2] B. Scrosati, J. Garche, Lithium batteries: Status, prospects and future, Journal of Power Sources, Volume 195, Issue 9, 2010, Pages 2419-2430, ISSN 0378-7753.

[3] C. G. Zosky, Handbook of Electrochemistry, Elsevier, 2007, ISBN-13: 978-0-444-51958-0.

[4] F.G. Hone, N.A, Tegegne,D.M. Andoshe, Advanced Materials for Energy Storage Devices, Electrode Materials for Energy Storage and Conversion; CRC Press: Boca Raton, 2021.

[5] Y. Zhong,Y. Ma,Q. Guo, et al., Controllable Synthesis of TiO_2@Fe_2O_3 Core-Shell Nanotube Arrays with Double-Wall Coating as Superb Lithium-Ion Battery Anodes, Sci Rep 7, 40927, 2017.

[6] J. Luo, et al., Rationally designed hierarchical TiO_2@Fe_2O_3 hollow nanostructures for improved lithium ion storage. Adv. Energy Mater. 2013, 3, 737–743.

[7] L. Besra, M. Liu, A review on fundamentals and applications of electrophoretic deposition (EPD), Progress in Materials Science, 52, Issue 1, 2007, Pages 1-61, ISSN 0079-6425.

[8] G. Kucinskis, G. Bajars, J. Kleperis, Graphene in lithium ion battery cathode materials: A review, Journal of Power Sources, 240, 2013, Pages 66-79, ISSN 0378-7753,

[9] H. Zhang, et al., Micro-structured Si@Cu_3Si@C ternary composite anodes for high performance Li-ion batteries, 2019, Ionics 25(10):4667–4673.

[10] D. Linden, T. B. Reddy, Handbook of Batteries, 3rd Edition. McGraw-Hill, 2002. ISBN 0-07-135978-8.

[11] H. Jung, M. Park, Y. G. Yoon, G. B. Kim, and S. K. Joo, Amorphous silicon anode for lithium-ion rechargeable batteries J. Power Sources, Seoul, vol. 115, pp. 346-351, April 2003.

[12] W. Xu, S. S. S. Vegunta, J. C. Flake, Surface-modified silicon nanowire anodes for lithium-ion batteries, Journal of Power Sources, 196, Issue 20, 2011, Pages 8583-8589, ISSN 0378-7753.

[13] M. Thakur, M. Isaacson, S. L. Sinsabaugh, M. S. Wong, S. L. Biswal, Gold-coated porous silicon films as anodes for lithium ion batteries, Journal of Power Sources, Volume 205, 2012, Pages 426-432, ISSN 0378-7753.

[14] B. Fuchsbichler, C. Stangl, H. Kren, F. Uhlig, S. Koller, High capacity graphite–silicon composite anode material for lithium-ion batteries, Journal of Power Sources, Volume 196, Issue 5, 2011, Pages 2889-2892, ISSN 0378-7753.

[15] P. M. Dziewoński, M. Grzeszczuk, Lithium ion intercalation in partially crystalline TiO_2 electrodeposited on platinum from aqueous solution of titanium (IV) oxalate complexes, Journal of Power Sources, Volume 190, Issue 2, 2009, Pages 545-552, ISSN 0378-7753.

[16] F. Wu, et al., A novel method to synthesize anatase TiO_2 nanowires as an anode material for lithium-ion batteries, Journal of Alloys and Compounds, Volume 509, Issue 8, 2011, Pages 3711-3715, ISSN 0925-8388.

[17] Y. Wang, et al., Facile Synthesis of Fe_2O_3-graphite Composite with Stable Electrochemical Performance as Anode Material for Lithium Ion Batteries, Electrochimica Acta, Volume 125, 2014, Pages 421-426, ISSN 0013-4686.

[18] S.K. Yadav, J.W. Cho, Functionalized Graphene Nanoplatelets for Enhanced Mechanical and Thermal Properties of Polyurethane Nanocomposites, 2013, Applied Surface Science, 266, 360-367.

[19] Y. Yuan, et al., Understanding materials challenges for rechargeable ion batteries within situ transmission electron microscopy. Nat Commun 8, 15806, 2017.

[20] A. Eftekhari, Low voltage anode materials for lithium-ion batteries, Energy Storage Materials, 7, 2017, Pages 157-180, ISSN 2405-8297.

[21] S.B. Chikkannanavar, D.M. Bernardi, L. Liu, A review of blended cathode materials for use in Li-ion batteries. J. Power Sources 2014, 248, 91–100.

[22] Y. Mekonnen, A. Sundararajan and A. I. Sarwat, A review of cathode and anode materials for lithium-ion batteries, SoutheastCon 2016, Norfolk, VA, USA, 2016, pp. 1-6.

[23] Y. Zhang, et al., High-energy cathode materials for Li-ion batteries: A review of recent developments. Sci. China Technol. Sci. 58, 1809–1828, 2015.

[24] C. Daniel, D. Mohanty, J. Li, D. L. Wood, Cathode materials review, AIP Conference Proceedings 16 June 2014; 1597 (1): 26–43.

[25] D. Wang, D. Choi, et al., Self-assembled TiO_2-graphene hybrid nanostructures for enhanced Li-ion insertion, ACS Nano 3 (4), 2009, 907–914.

[26] J. H. Kwon, et al., Reversible Conversion Reactions of Mesoporous Iron Oxide with High Initial Coulombic Efficiency for Lithium-ion Batteries." ACS sustainable chemistry & engineering, v. 9,.49 pp. 16627-16636.

[27] B.L. Dasari, et al., Graphene and derivatives – Synthesis techniques, properties, and their energy applications. Energy. 140, 766-778, 2017.

[28] H. Dong, et al., An overview on limitations of TiO_2-based particles for photocatalytic degradation of organic pollutants and the corresponding countermeasures, Water Research, Volume 79, 2015, Pages 128-146, ISSN 0043-1354.

[29] H. Liu, et al., Synthesis of $TiO_2/SiO_2@Fe_3O_4$ magnetic microspheres and their properties of photocatalytic degradation dyestuff, Catalysis Today, Volume 175, Issue 1, 2011, Pages 293-298, ISSN 0920-586.

[30] M.N. Tahir, et al., Extraordinary Performance of Carbon-Coated Anatase TiO_2 as Sodium-Ion Anode. Adv Energy Mater. 2016 Feb;6(4):1501489.

[31] A. Wanag, et al., Influence of rGO and Preparation Method on the Physicochemical and Photocatalytic Properties of TiO_2/Reduced Graphene Oxide Photocatalysts, Catalysts 2021, 11, 1333.

[32] I.S. Ahmed, M.S. Sanad, Maghemite-based anode materials for Li-Ion batteries: The role of intentionally incorporated vacancies and cation distribution in electrochemical energy storage, Journal of Alloys and Compounds, Volume 861, 2021, 157962, ISSN 0925-8388.

[33] M. Madian, A. Eychmüller,L. Giebeler, Current Advances in TiO_2-Based Nanostructure Electrodes for High Performance Lithium Ion Batteries. Batteries 2018, 4, 7.

[34] H. Xia, W. Xiong, C.K. Lim, et al., Hierarchical TiO_2-B nanowire@α-Fe_2O_3 nanothorn core-branch arrays as superior electrodes for lithium-ion microbatteries. Nano Res. 7, 1797–1808 (2014).

[35] J. Chen, X. Hu, H. Gao, S. Yan, S. Chen, X. Liu, Graphene-wrapped $MnCO_3$/Mn_3O_4 nanocomposite as an advanced anode material for lithium-ion batteries: Synergistic effect and electrochemical performances, Journal of Materials Science & Technology, Volume 99, 2022, Pages 9-17, ISSN 1005-0302.

[36] R. A. Adams, et al., Binder Free N- and O-Rich Carbon Nanofiber Anodes for Long Cycle Life K-Ion Batteries, ACS Applied Materials & Interfaces, 2017; 9, 17872–17881.

[37] B. Tian, et al., Insight into lithium diffusion in conversion-type iron oxide negative electrode, 2015, J. Phys. Chem., C 119:919–925.

[38] S. Lee, W. Eom, H. Park, and T. H. Han, High-Temperature Stable Anatase Titanium Oxide Nanofibers for Lithium-Ion Battery Anodes, ACS Applied Materials & interfaces, 2017, 9 (30), 25332-25338.

[39] X.H. Rui, N. Yesibolati, S.R. Li, C.C. Yuan, C.H. Chen, Determination of the chemical diffusion coefficient of Li^+ in intercalation-type $Li_3V_2(PO_4)_3$ anode material, Solid State Ionics, Volume 187, Issue 1, 2011, Pages 58-63, ISSN 0167-2738.

[40] I.S. Lyubutin, A.O. Baskakov, S.S. Starchikov, Kun-Yauh Shih, Chun-Rong Lin, Yaw-Teng Tseng, Shou-Shiun Yang, Zhen-Yuan Han, Yu.L. Ogarkova, V.I. Nikolaichik, A.S. Avilov, Synthesis and characterization of graphene modified by iron oxide nanoparticles, Materials Chemistry and Physics, Volume 219, 2018, Pages 411-420, ISSN 0254-0584.

[41] S. Hillier, Accurate quantitative analysis of clay and other minerals in sandstones by XRD: Comparison of a Rietveld and a reference intensity ratio (RIR) method and the importance of sample preparation. Clay Miner. 2000, 35, 291–302.

[42] X. Zhou, et al., XRD-based quantitative analysis of clay minerals using reference intensity ratios, mineral intensity factors, Rietveld, and full pattern summation methods: A critical review, Solid Earth Sci. 2018, 3, 16–29.

[43] N. Kumar and V.C. Srivastava, Simple Synthesis of Large Graphene Oxide Sheets via Electrochemical Method Coupled with Oxidation Process, Department of Chemical Engineering, Indian Institute of Technology Roorkee, Roorkee 247667, Uttarakhand, India, ACS Omega 2018, 3, 10233−10242.

[44] H. Xu, et al., A new nano-mineral of Fe_2O_3 polymorph with giant coercive field, American Mineralogist 102, 2017, 711 - 719.

[45] H. Xia, W. Xiong, C,K. Lim, et al., Hierarchical TiO_2-B nanowire@α-Fe_2O_3 nanothorn core-branch arrays as superior electrodes for lithium-ion microbatteries. Nano Res. 7, 1797–1808 (2014).

[46] K. Huang, L. Chen, J. Deng, J. Xiong, Enhanced Visible-Light Photocatalytic Performance of Nanosized Anatase TiO_2 Doped with CdS Quantum Dots for Cancer-Cell Treatment, Journal of Nanomaterials, vol., 2012, Article ID 720491, 12 pages.

[47] L. Zuniga, et al., Centrifugally Spun α-Fe_2O_3/TiO_2/Carbon Composite Fibers as Anode Materials for Lithium-Ion Batteries. Appl. Sci. 2019, 9, 4032.

[48] S. Li, et al., Bio-Inspired Hierarchical Nanofibrous Fe_3O_4-TiO_2-Carbon Composite as a High-Performance Anode Material for Lithium-Ion Batteries. ACS Appl. Mater. Interfaces 2016, 8, 17343–17351.

[49] L. Gao, et al., Hierarchical 3D TiO_2@Fe_2O_3 nanoframework arrays as high-performance anode materials. Nanoscale 2014, 6, 6463–6467.

[50] Y. Fu, et al., Sun, S. Stem-like nano-heterostructural MWCNTs/α-Fe_2O_3@TiO_2 composite with high lithium storage capability. J. Alloys Compd. 2016, 684, 419–427.

[51] T.G. Qin, et al., Fabrication of Fe_2O_3@TiO_2 core-shell nanospheres as anode materials for lithium-ion batteries. J. Mater. Sci.-Mater. Electron. 2018, 29, 12944–12950.

[52] M. Liang, J. Zou, X. Zeng, W. Ding, Nanostructured Fe_2O_3 Based Composites Prepared through Arc Plasma Method as Anode Materials in the Lithium-Ion Battery, Journal of Nanomaterials, 2016, art. no. 1207907.

[53] L.Y. Beaulieu, et al., Reaction of Li with grain-boundary atoms in nanostructured compounds. J. Electrochem. Soc. 147, 3206–3212, 2000.

[54] S. Laruelle, et al. On the origin of the extra electrochemical capacity displayed by MO/Li cells at low potential. J. Electrochem. Soc. 149, A627–A634, 2002.

[55] P. Balaya, et al., Fully reversible homogeneous and heterogeneous Li storage in RuO_2 with high capacity. Adv. Funct. Mater. 13, 621–625, 2003.

[56] H. Li, P. Balaya, J. Maier, Li-storage via heterogeneous reaction in selected binary metal fluorides and oxides. J. Electrochem. Soc. 151, A1878–A1885, 2004.

[57] H. Li, G. Richter, J. Maier, Reversible formation, and decomposition of LiF clusters using transition metal fluorides as precursors and their application in rechargeable Li batteries. Adv. Mater. 15, 736–739, 2003.

[58] S. Guo, S. Wang, N. Wu, J. Liu, Y. Nic, W. Liu, Facile synthesis of porous Fe_2TiO_5 microparticulates serving as anode material with enhanced electrochemical performances, RSC Adv. 5, 2015, 103767e103775.

[59] S. Guo, et al., Porous TiO_2–$FeTiO_3$@Carbon nanocomposites as anode for high-performance lithium-ion batteries, Journal of Alloys and Compounds, Volume 858, 2021, 157635, ISSN 0925-8388.

[60] Y. Yang, et al., Enhanced electrochemical performance of alpha-Fe_2O_3 grains grafted onto TiO2-Carbon nanofibers via a Vapor-Solid reaction as anode materials for Li-Ion batteries. Appl. Surf. Sci. 2019, 463, 322–330.

[61] K. Redel, et al., Origin of extra capacity in advanced Li–Rich cathode materials for rechargeable Li–Ion batteries, Chemical Engineering Journal, Volume 424, 2021, 130293, ISSN 1385-8947.

[62] K. Thanapalan, M. Bowkett, J. Williams, M. Hathway, T. Stockley, Advanced EIS Techniques for Performance Evaluation of Li-ion Cells, IFAC Proceedings Volumes, Volume 47, Issue 3, 2014, Pages 8610-8615, ISSN 1474-6670.

[63] S. Hink, et al., Impedance Spectroscopic Investigation of Proton Conductivity in Nafion Using Transient Electrochemical Atomic Force Microscopy (AFM), Membranes, 2012, 2, 237-252.

[64] Y. Yang, et al., Enhanced electrochemical performance of α-Fe_2O_3 grains grafted onto TiO_2-Carbon nanofibers via a vapor-Solid reaction as anode materials for Li-Ion batteries, Applied Surface Science, Volume 463, 2019, Pages 322-330.

[65] H. Xia, et al., Hierarchical TiO_2-B nanowire@α-Fe_2O_3 nanothorn core-branch arrays as superior electrodes for lithium-ion microbatteries. Nano Res. 7, 1797–1808.

[66] A. Casimir, et al., Silicon-based anodes for lithium-ion batteries: Effectiveness of materials synthesis and electrode preparation, Nano Energy, Volume 27, 2016, Pages 359-376, ISSN 2211-2855.

[67] N. Srivastava, et al., Electrochemical performance of Li-rich NMC cathode material using ionic liquid based blend polymer electrolyte for rechargeable Li-ion batteries, Journal of Alloys and Compounds, Volume 843, 2020, 155615, ISSN 0925-8388.

[68] Q. Li, J. Chen, L. Fan, X. Kong, Y. Lu, Progress in electrolytes for rechargeable Li-based batteries and beyond, Green Energy & Environment, Volume 1, Issue 1, 2016, Pages 18-42, ISSN 2468-0257.

PUBLICITY OF THE AUTHOR

The Hirsch citation index of the author's publications is 4, with a total of 5 publications in the SCOPUS database.

Publications related to the content of thesis:

- **K. Kaprans,** J. Mateuss, A. Dorondo, G. Bajars, G. Kucinskis, P. Lesnicenoks, Electrophoretically deposited α-Fe_2O_3 and TiO_2 composite anchored on rGO with excellent cycle performance as anode for lithium-ion batteries. Solid State Ionics 319, 1-6 (2018), (Cited 23 times). https://doi.org/10.1016/j.ssi.2018.01.042
- **K. Kaprans**, G. Bajars, G. Kucinskis, A. Dorondo, J. Mateuss, J. Gabrusenoks, Electrophoretic Nanocrystalline Graphene Film Electrode for Lithium Ion Battery, IOP Conference Series: Materials Science and Engineering 77 (1), 012042 (2015), (Cited 6 times). https://iopscience.iop.org/article/10.1088/1757-899X/77/1/012042

Publications less relevant to the topic of thesis:

- G.Kucinskis, G.Bajars, K.Bikova, **K.Kaprans**, J.Kleperis, Microstructural Influence on Electrochemical Properties of $LiFePO_4$/C/Reduced Graphene Oxide Composite Cathode, Russian Journal of Electrochemistry 55, 517-523 (2019).
- A. Plavniece, A. Volperts, G. Dobele, A. Zhurinsh, **K. Kaprans**, I. Kruusenberg, Wood and black liquor-based N-doped activated carbon for energy application, Sustainability 13 (16), 923, (2021).
- P. Lesnicenoks, M. Zvine, A. Januskevica, V.L. Muzikants, M.K. Jurjans, **K. Kaprans**, A. Volperts, G. Kucinskis, G. Bajars, G. Dobele, J. Kleperis, Nanostructured carbon materials as promoters of energy storage, Bulgarian Chemical Communications 48, 365-372, (2016).

PARTICIPATION IN CONFERENCES

- **K. Kaprans,** Synergistic Behaviour of TiO_2/Fe_2O_3/rGO Ternary Nanocomposite as Anode for Lithium-Ion Battery" Scholars Frontiers in Nanoscience and Nanotechnology Congress" NANOTEK2023, 2023, London, Great Britain, March 27 -28.
- **K. Kaprans,** G. Bajars, G. Kucinskis, Investigation of Fe_2O_3 and TiO_2 molar ratio impact on lithium – ion battery electrode performance, international conference on batteries - BATTERIES EVENT 2022, October 18-21, 2022.
- **K. Kaprans,** Synergistic behaviour of TiO_2/ Fe_2O_3/rGO ternary nanocomposite as Anode for Lithium - Ion batteries, 7th International Conference on Multifunctional, Hybrid and Nanomaterials (HYMA -2022), October 19-22, 2022, Genoa, Italy, Available at SSRN: https://ssrn.com/abstract=4240892.
- **K. Kaprans,** A. Volperts, G. Bajars, G. Kucinskis, G. Dobele, J. Kleperis, Nanostructured porous hybrid network of nitrogen-doped carbon as anode for Li-ion batteries, Functional Materials and Nanotechnologies, Vilnius, Lithuania, November 23-26, 2020, Book of Abstracts p.76
- G.Bajars, G.Kucinskis**, K. Kaprans**, J.Kleperis, Recent developments of electrode materials for lithium – ion batteries, 16th International Symposium on Systems with Fast Ionic Transport, Chernogolovka, Russia, 2018, Book of Abstracts: p. 47
- **K. Kaprans,** J. Mateuss, A. Dorondo, G. Bajars, J. Kleperis, Nanostructured Fe_2O_3, TiO_2 and reduced graphene oxide with excellent electrochemical performance as anode material for lithium ion batteries, COST TO-BE - FALL-2017, Riga, Latvia, June 11–13, 2017.
- **K.Kaprans**, J.Mateuss, A. Dorondo, G.Bajars, J. Kleperis, Electrophoretically deposited α-Fe_2O_3 and TiO_2 composite anchored on rGO with excellent cycle performance as anode for lithium - ion batteries, 21st International Conference on Solid State Ionics, Padua, Italy, June 18-23, 2017, Book of Abstracts p.222
- **K. Kaprans**, J. Mateuss, A. Dorondo, G. Bajars, G.Kucinskis, J. Kleperis, Electrophoretically deposited graphene oxide/TiO_2 and ultrasmall Fe_2O_3 nanoparticles thin film composite as anode for highperformance lithium ion batteries, 12th International Symposium of Systems with Fast ionics transport (ISSFIT -12), Kaunas, Lithuania, July 3-7, 2016.
- **K. Kaprans,** G. Bajars, A. Dorondo, J.Mateuss, G. Kucinskis, J. Gabrusenoks, J. Kleperis, A. Lusis, Electrophoretic Graphene Film Electrode for Lithium Ion Battery, Joint 12th Russia/CIS/Baltic/Japan Symposium on Ferroelectricity and 9th International Conference Functional Materials and Nanotechnologies, September 29 – October 2 Riga, 2014, Book of Abstracts p.410
- Annual scientific conferences of the Institute of Solid State Physics, University of Latvia (2014-2021).

SCIENTIFIC PROJECTS

The thesis is related to the following research projects:

1. "Strengthening the Capacity of the Doctoral Studies of the University of Latvia in the Framework of the New Doctoral Studies Model" No. 8.2.2.0/20/I/006, 01.07.2021.-31.10.2023.
2. Latvian Council of Science basic and applied research project No lzp-2020/1-0425 "Life cycle prediction of lithium-ion battery electrodes and cells using current and voltage measurements", 2021-2023.
3. Nanostructured nitrogen-doped carbon materials as enablers for energy harvesting and storage technologies, 2018-2021, NN-CARMA.
4. UL ISSP Students and Young Scientists Project Nr. SJZS/2020/9, 2020.
5. H2020 SPIRE project, "Electrocatalytic synthesis of ethylene oxide from CO2" (COEXIDE), 2018 -2019.
6. A/S Sidrabe and National Competence Centre project, Applications of lithium vaccum coatings in battery anode materials, 2018 - 2019.
7. Latvian Council of Science Cooperation Project "Synthesis and Research of Controlled Porosity Composite Materials for Thin Layers and their Systems for Energy Storage and Conversion Applications", Project No. 666/2014, 2014 - 2018.

The Institute of Solid State Physics of the University of Latvia as a Centre of Excellence has received support from the European Union's Horizon 2020 call H2020-WIDESPREAD-01-2016-2017-TeamingPhase2 project CAMART2, contract No 739508.

ACKNOWLEDGEMENTS

I would like to express my gratitude to supervisor of the work, Dr. chem. Gunārs Bajārs for his immeasurable help in development of the thesis, providing valuable advice on both the planning of results and analysis and interpretation of the data. His immense knowledge, plentiful experience and continuous support have encouraged me in all the time of my research and daily life. I am genuinely grateful for possibility to work under his leadership.
The head of laboratory, Dr. phys. Gints Kučinskis for his valuable advice and motivation to continue this work.
Reinis Ignatāns and Liga Ignatāne for advice on interpretation of X-ray structural analysis data.
Many thanks also to other colleagues of the Laboratory for Energy Harvesting and Storage.
Līga Britāla for SEM and EDX measurements.
Kārlis Kundziņš for SEM images.
Ingaras Lukoševičas for XPS measurements.
Evgeny Gabrusenok for Raman spectra measurements.
I want to thank God for the opportunity and guidance to achieve my goals and succeed.
I would like to thank my mum and dad for raising me and for their tireless efforts and support to achieve my dreams and goals.
I would like to thank my wife Ruth and sons Jacob, Karl and newborn daughter Marta for their patience and understanding during the dissertation process.
I would like to thank the Institute of Solid State Physics for being a nice place where to work and develop my career. Additionally, I would like to acknowledge Scientific Research Project for Students and Young Researchers Nr. SJZS/2020/9, 2020 realized at the Institute of Solid-State Physics, University of Latvia.

Funding for the development of doctoral thesis was received from the grant project "**Strengthening of the capacity of doctoral studies at the University of Latvia within the framework of the new doctoral model**", identification No. 8.2.2.0/20/I/006

LATVIJAS UNIVERSITĀTE

NACIONĀLAIS ATTĪSTĪBAS PLĀNS 2020

EIROPAS SAVIENĪBA
Eiropas Sociālais fonds

IEGULDĪJUMS TAVĀ NĀKOTNĒ